Euclid payload module: telescope characteristics and technical challenges

Luis Gaspar Venancio, René Laureijs, Jose Lorenzo, J. Salvignol, Alex Short, et al.

Luis M. Gaspar Venancio, René Laureijs, Jose Lorenzo, J. C. Salvignol, Alex Short, Paolo Strada, Roland Vavrek, Ludovic Vaillon, Corrado Gennaro, Jerome Amiaux, Éric Prieto, "Euclid payload module: telescope characteristics and technical challenges," Proc. SPIE 9143, Space Telescopes and Instrumentation 2014: Optical, Infrared, and Millimeter Wave, 91430I (2 August 2014); doi: 10.1117/12.2054768

SPIE.

Event: SPIE Astronomical Telescopes + Instrumentation, 2014, Montréal, Quebec, Canada

Euclid payload module : telescope characteristics and technical challenges

Luis M. Gaspar Venancio*[a], René Laureijs[a], Jose Lorenzo[a], J.C. Salvignol[a], Alex Short[a], Paolo Strada[a], Roland Vavrek[a], Ludovic Vaillon[b], Corrado Gennaro[c], Jerome Amiaux[d], Éric Prieto[e]
[a]European Space Agency (ESA/ESTEC), Keplerlaan 1, Noordwijk 2200AG, The Netherlands; [b]Airbus Defense and Space, 31 r. des Cosmonautes, 31402 Toulouse, France; [c]Thales Alenia Space Italia, via Saccomuro, 00131 Roma, Italy; [d] CEA/Service d'Astrophysique, Orme des Merisiers Bat.109, 91191 Gif sur Yvette, France; [e]Laboratoire d'Astrophysique de Marseille, 38 r. Frédéric Joliot-Curie, 13388 Marseille Cedex 13, France

ABSTRACT

Euclid is an European Space Agency (ESA) mission to map the geometry of the dark Universe. The mission will investigate the distance-redshift relationship and the evolution of cosmic structures. It will achieve this by measuring shapes and redshifts of galaxies and clusters of galaxies out to redshifts ~2, equivalent to 10 billion years back in time. Euclid will make use of two primary cosmological probes, in a wide survey over the full extragalactic sky : the Weak Gravitational Lensing (WL) and Baryon Acoustic Oscillations (BAO). The main goal of the Euclid payload module (PLM) is to provide high quality imaging of galaxies and accurate measurement (less than 0.1%) of galaxies redshift over a large field of view (FoV). The present paper focuses on the telescope of the PLM excluding the instruments. We present a brief introduction to the Euclid PLM system and will report how the constraints of each instrument have driven the definition of the telescope-to-instrument optical interfaces. Furthermore we introduce the description of the telescope optical characteristics and report its nominal performances. Finally, the technical challenges to be faced by ESA's industrial partners are underlined.

Keywords: Euclid, telescope, payload, optics, performance

1. INTRODUCTION

1.1 Euclid mission scientific background

Euclid is a survey mission designed to understand the origin of the Universe's expansion rate (see Figure 1). It will use cosmological probes to investigate the nature of dark energy, dark matter and gravity by tracking their observational signatures on the geometry of the universe and on the cosmic history of structure formation. The mission is optimized for two independent primary cosmological probes: Weak gravitational Lensing (WL) and Baryonic Acoustic Oscillations (BAO)[1].

*luis.miguel.gaspar.venancio@esa.int; phone +31 (0)71 565 8054; www.esa.int

Space Telescopes and Instrumentation 2014: Optical, Infrared, and Millimeter Wave, edited by Jacobus M. Oschmann, Jr., Mark Clampin, Giovanni G. Fazio, Howard A. MacEwen, Proc. of SPIE Vol. 9143, 91430I · © 2014 SPIE
CCC code: 0277-786X/14/$18 · doi: 10.1117/12.2054768

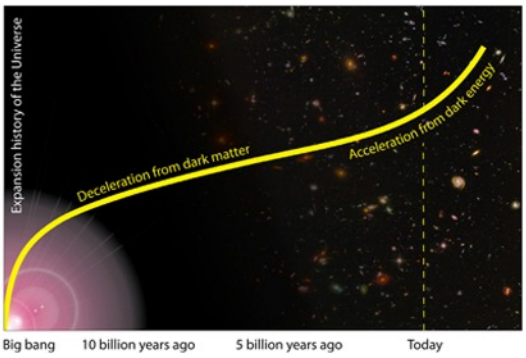

Figure 1. Expansion history of the Universe[3].

The WL is the signature of a mass perturbing the light paths between the observed object and the observer. The WL produces a shape change in the image of a galaxy, typically a stretching along one direction (see Figure 1). For very weak lensing such stretch is imperceptible in images of individual sources but can be measured by observation of large number of sources in the same field of view (FoV) and statistical analysis[2]. The lensing signal is derived from the calculation of the shape and distance of all the objects observed in the survey. The WL signal accuracy is thus driven by the image quality level and uniformity of the telescope[5] over the FoV but also by its stability over time.

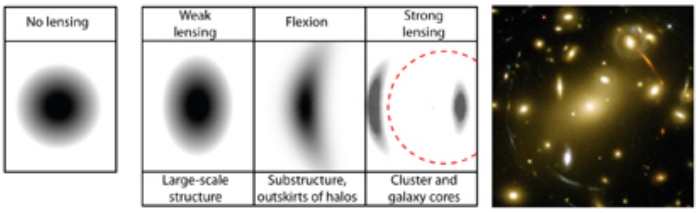

Figure 2. Illustration of the effect of a lensing mass on a circularly symmetric image[3].

The BAOs are wiggle patterns, imprinted in the clustering of galaxies. The BAO probe relies on the mapping of the galaxies distribution in three dimensions by measuring their spectroscopic redshift. The amplitude, shape and anisotropy within the power spectrum of the galaxies distribution contains information on the structure growth and expansion histories of the Universe[1].

To achieve the challenging scientific goals, tens of millions of galaxies need to be observed. The survey itself will cover 15000 deg^2 of the sky observed from the Earth's Lagrange point L2.

1.2 An overview on the PayLoad Module (PLM)

The two probes are implemented with two instruments in the PLM. The VISible imager (VIS) and the Near Infared Spectrometer and Photometer (NISP). The Table 1 recalls the requirements for each instrument.

Table 1. PLM instruments main optical design driving requirements

Parameter	Units	Values				
Instrument		VIS	NISP			
FoV	deg^2	0.787×0.709	0.763×0.722			
Capability		Imaging	Imaging photometry (NIP)			Spectroscopy (NIS)
Spectral range	nm	550-900	920-1192	1192-1544	1544-2000	1100-2000
Plate scale	arcsec/pixel	0.1	0.3			
Resolving power		Not applicable	Not applicable			250
Sensitivity		m_{AB} = 24.5	m_{AB}= 24			3e-16 erg.cm^{-2}.s^{-1}

The VIS instrument includes a focal plane, a read-out shutter and a calibration unit. The telescope images the sky directly on the VIS focal plane. The NISP instrument is more complex. It has a single detectors array for both photometric and slitless spectroscopy mode. A filter wheel and a grating wheel are included in NISP. The plate scale is achieved with six lenses re-imaging the telescope focal plane on the NISP focal plane. The NISP also includes its own calibration unit. The Figure 3 gives an external view of the NISP instrument.

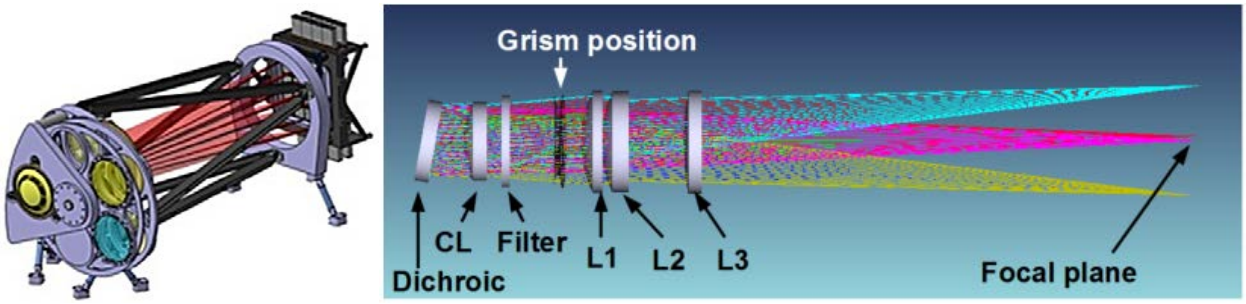

Figure 3. (Left) NISP instrument overview[6]. (Right) NISP optical ray tracing including the telescope dichroic[4].

Both instruments are optically interfaced with an unique telescope via a dichroic plate, located at the telescope exit pupil, performing the spectral split between the VIS and the NISP as shown in Figure 4. The telescope and both instruments are mechanically mounted on a common optical bench. The large FoV leads to a Korsch-type three-mirror anastigmat telescope. For both instruments the mode of observation is step-and-stare and the stability of the telescope Line of Sight (LoS) must be ensured with a very high accuracy. During one observation, the drift of the telescope LoS due to residual motions of the spacecraft is monitored by two Fine Guidance Sensors (FGS) located on the same plane as the VIS instrument focal plane.

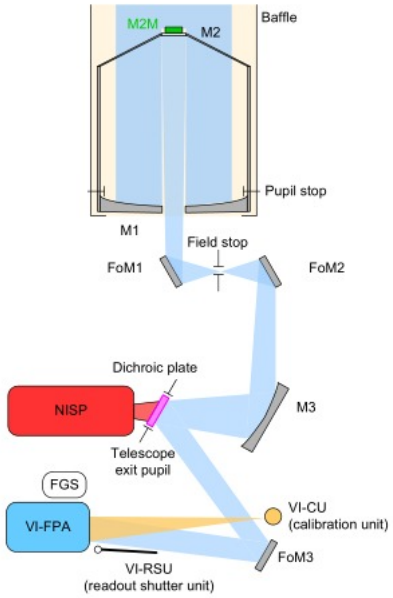

Figure 4. PLM schematics.

In the following pages, the focus is put on the telescope. Its development, including the dichroic plate, is on-going under the responsibility of Airbus Defense & Space (Airbus) in France. The Euclid industrial consortium is led by Thales Alenia Space Italy (TAS-I) acting as prime contractor.

2. TELESCOPE MAIN REQUIREMENTS

2.1 VIS channel specific image quality metrics

The weak lensing experiment leads to specific metrics unusual in the definition of optical systems. In Euclid mission the Point Spread Function (PSF) is not only characterized by the Full Width at Half Maximum (FWHM), the Encircled Energy radius (EE) at 50% (EE50) and 80% (EE80) of maximum but also by additional quantities referred to as R^2 and the ellipticity *e*. Those two quantities are commonly used by the WL scientific community, but less in the optical engineering community.

The metrics *e* and R^2 are based on the second moments of the PSF considered as a function $PSF(\boldsymbol{X})$ of the spatial variable $\boldsymbol{X}$. The moments include a weighting with a Gaussian function *w* defined by :

$$w(\boldsymbol{X}) = \frac{1}{(2\pi\sigma^2)} \exp\left[-\frac{1}{2\sigma^2}\{(x_1 - x_1^{cen})^2 + (x_2 - x_2^{cen})^2\}\right] \quad (1)$$

with (x_1^{cen}, x_2^{cen}) the PSF centroid coordinates and σ =0.75 arcsec. The value of σ corresponds to the typical size of the galaxies to be observed. The quadrupole moments of the function $PSF(\boldsymbol{X})$ are then defined as a matrix, each term Q_{ij} in the matrix being given by the equation (2).

$$Q_{ij} = \frac{1}{F(0)} \int w(\boldsymbol{X}) \times (x_i - x_i^{cen}) \times \left(x_j - x_j^{cen}\right) \times PSF(\boldsymbol{X}) d^2\boldsymbol{X} \quad (2)$$

with $F(0)$ being the zero[th] order moment of the PSF($\mathbf{X}$) and defined by:

$$F(0) = \int w(\boldsymbol{X}) \times PSF(\boldsymbol{X}) d^2\boldsymbol{X} \quad (3)$$

The ellipticity *e* and R^2 are then defined as follow:

$$e = \sqrt{\frac{(Q_{11} - Q_{22})^2 + (2Q_{12})^2}{(Q_{11} + Q_{22})^2}} \quad (4)$$

$$R^2 = Q_{11} + Q_{22} \quad (5)$$

The metric *e* is a measure of the weighted PSF stretch, while R^2 is a measure of its size. Both metrics are designed to capture the minute asymmetry within PSFs similar to the one in Figure 5.

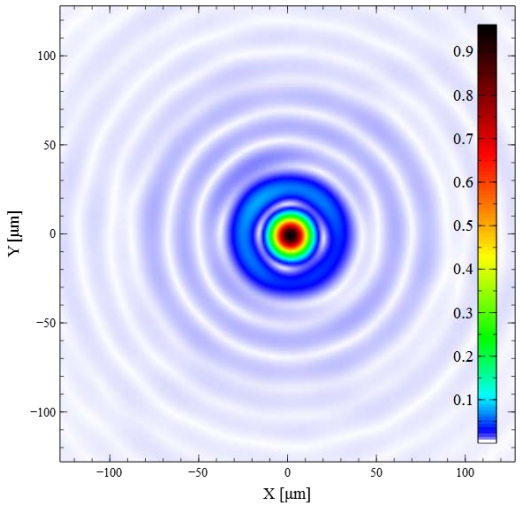

Figure 5. Typical PSF of the Euclid telescope as optimized at ambient. A square root scale is used to enhance the PSF asymmetry.

2.2 Main driving requirements

This paragraph focuses mainly on the spectral and PSF metrics requirements. The overall optical requirements are defined in Table 1.

Table 2. Main requirements for the PSF metrics in telescope VIS channel.

Parameter	Value
e	< 14%
$\delta e/e$ (stability of e)	$< 2\text{x}10^{-3}$
R^2 (defined for λ=800nm)	< 0.055 arcsec^2
$\delta R^2/R^2$ (stability of R^2)	$< 2\text{x}10^{-3}$
FWHM	<0.155 arcsec

The level of straylight and the ghosts must be well controlled. In fact, for bright objects the straylight and ghost irradiance per pixel, if too high, may reduce the number of objects available per field, thus effectively reducing the number of galaxies available for analysis. The straylight generated by the telescope in both channels is thus limited to 10% of the zodiacal background and the contrast ratio between ghost and the image must be lower than 5×10^{-5} averaged over the band 400-1600 nm for the VIS channel and 5×10^{-5} over each photometer and spectroscopic bands for the NISP channel.

For the same reason, the out-of-band throughput of the telescope must be lower than 0.09% in average for the band between 400nm to 525nm, and lower than 0.16% in average for the band 935nm to 1600nm.

For the NISP channel the requirements defined are the EE50 and EE80. The values applicable to the Euclid spacecraft (excluding the NISP instrument contribution) are in Table 3.

Table 3. Encircled energy radii at 50% and 80% for the telescope's NISP channel.

Wavelength [nm]	EE80 [arcsec]	EE50 [arcsec]
2000	0.680	0.297
1800	0.621	0.282
1720	0.597	0.273
1486	0.529	0.252
1259	0.469	0.234
1173	0.447	0.226
1033	0.416	0.211

All the metrics are defined in the sky in arc second units, the function $PSF(\boldsymbol{X})$ is defined in the telescope plane. For the purpose of this paper the metrics are calculated using the paraxial focal length for the projection from the sky on the telescope focal plane and backward. The Gaussian weighting function is thus defined in the telescope focal plane by σ = 89.08 μm. The metrics e, R^2, EE50 and EE80 once calculated on the focal plane are projected back in the sky using the paraxial focal length.

3. TELESCOPE DESCRIPTION, SPECTRAL AND IMAGING PERFORMANCE

3.1 Telescope description

To achieve high image quality over the FoVs defined in Table 1 a Korsch type telescope has been designed in the early phases of the Euclid project and is the baseline for the PLM Preliminary Design Review (PDR) held in April 2014. The paraxial focal length is f = 24.5 meters and the telescope entrance pupil has a diameter of 1.2 meter. To cope with any

disturbance in the image quality after launch, the secondary mirror M2 is equipped with a mechanism (M2M) with three degrees of freedom for the adjustment in-flight of its position in focus & in tilt. The Figure 6 shows the optical lay-out of the telescope with the VIS, NISP and FGS channels. Three flat mirrors (FOM1 to FOM3) are used to fold the optical combination below the optical bench: FOM1 & FOM2 are between M2 and M3, while FOM3 is between the dichroic plate and the VIS focal plane.

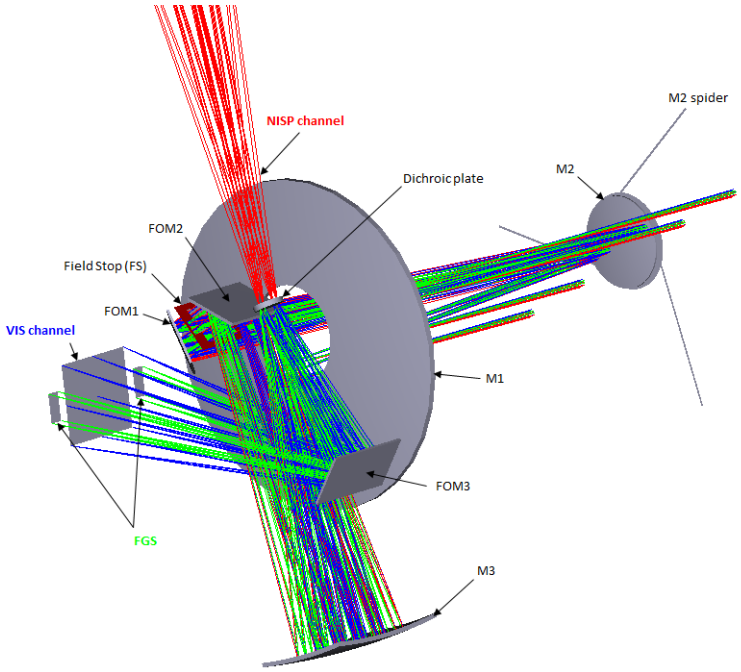

Figure 6. Telescope ray-tracing showing the light beams for the VIS, NISP and FGS channels.

The off-axis FoV creates an obscuration in M1 larger than the projected shadow of the M2 (including its baffle). The size and shape of the central obscuration is optimized such as to minimize the impact on e and R^2.

For improved stability, the whole telescope, including the mirrors and structure, is entirely made out of a single material: sintered Silicon Carbide (SiC). SiC combines a high stiffness, low density and high thermal conductivity thus reducing thermal gradients along and across the optical path. The Ø1.25 m primary mirror (M1) is monolithic, while the large optical bench is made of four different SiC parts brazed together. A major advantage of this single-material telescope is the homothetic shrinkage during the cool-down to the cold operating temperature of 125 K. Second-order effects due to interfaces, mirrors coating and gradient across the telescope structure are compensated by small adjustments of the M2 tilt and focus.

The NISP and VIS channels are separated by a dichroic plate located close to the FOM2 on the exit pupil of the telescope. The dichroic is one of the most critical components due to its size (larger than 110 mm in diameter) but also to its stringent requirements on WFE and spectral reflectance/transmittance. The plate has a dichroic coating in the front face with a high reflectance in the VIS spectral band and an anti-reflection coating on the back surface for the NISP spectral band. A small wedge between the two surfaces enables the discrimination between the image reflected by the front face and the ghost in the VIS channel created by the back surface. The dichroic plate substrate is fused silica for low absorption in the near infra-red.

3.2 Spectral performance

The dichroic defines the spectral transition between the NISP and VIS channel. The transition zone is limited to 35 nm including all contributors (spectral shift with angle of incidence, layers thickness inhomogeneity,..). The spectral rejection out-of-band is achieved by using the dichroic and filters on the FOMs. FOM1 and FOM2 have high-pass filter and the FOM3 has a bandpass filter.

In the Phase A/B1 of the Euclid mission development a breadboarding activity of the dichroic plate was performed by Selex Galileo and funded by the ESA's Technology Research Program (TRP). The measured spectral performance are shown in Figure 7.

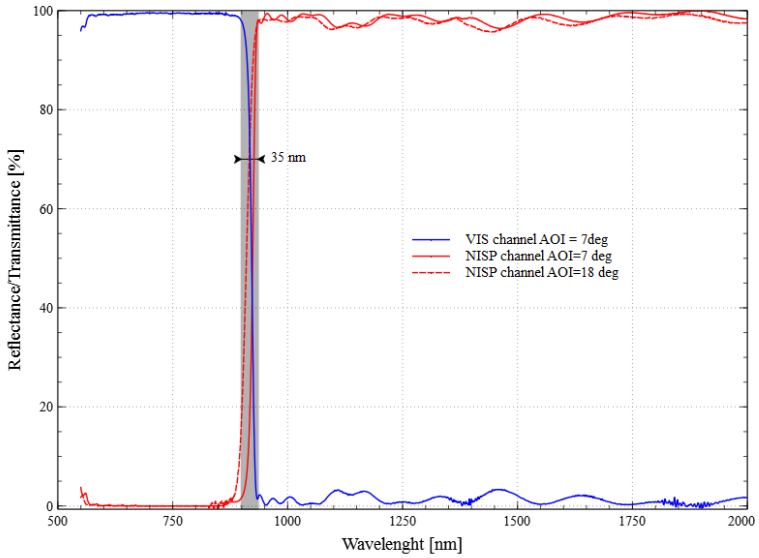

Figure 7. Measured reflectance and transmittance of the dichroic plate breadboard developed by Selex Galileo.

The excellent performance achieved by the breadboard has demonstrated the feasibility of the dichroic plate over the spectral range 500nm to 2000nm. Two dichroic Demonstrator Models (DM), with improved performances in terms of out-of-band rejection and spectral range as specified in 2.2, are being developed in parallel by industrial Optics Balzer Jena (OBJ) and AMOS with Schott-Switzerland..

By the time the present paper was written little information was available on the spectral performance for the FOMs' filters. For the dichroic, preliminary theoretical results were provided by OBJ and Schott. A first assessment of the telescope spectral relative throughput for both channels is presented in Figure 8. The curves are derived assuming the FOMs' spectral templates specified for manufacturing.

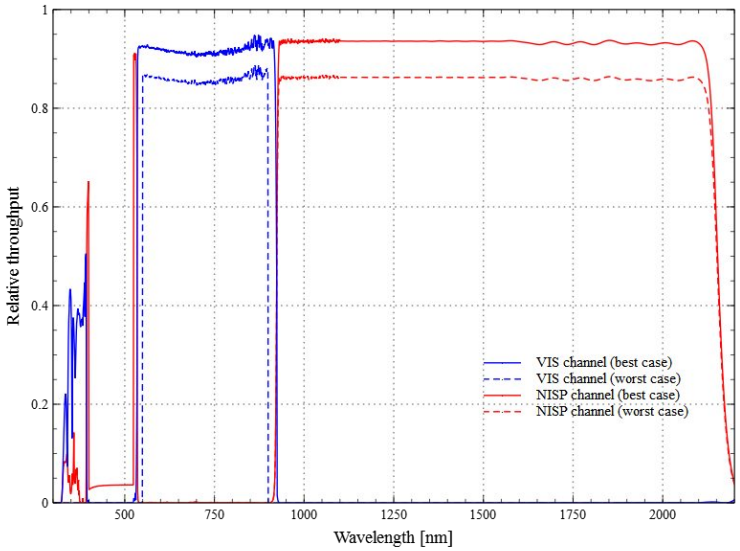

Figure 8. Theoretical telescope throughput for the VIS and NISP channel. The average angle of incidence (12 degrees) is considered.

All coatings are currently specified in the spectral 400nm to 2200 nm, explaining the high throughput in VIS channel for wavelengths lower than 400 nm. In addition to the steep slope at the VIS-NISP transition an additional requirement was added at system level to have a transition for the VIS channel between in-band and out-of-band reflectance smaller than 25 nm. The sharp transitions at 550 nm and 900 nm are necessary for the deconvolution of simulated PSFs from the images.

3.3 The telescope image quality in VIS channel

The PSF and the telescope pupil function are conjugated by Fourier Transform. One can immediately think of aberrations or Wave Front Error (WFE) as the main contributors to the PSF shape changes, however any obscuration of the pupil can also have an impact. An early analysis of the impact of the spider's struts curvature on e and R^2 has shown that the straight struts are not optimum for e neither is a half-circle spider struts (see Figure 7). The impact on R^2 is negligible (variation is about 5×10^{-4} arcsec^2). The metric R^2 is more sensitive to the diameter of the central obscuration. A perfect Euclid telescope was assumed with a spider centered on the telescope entrance pupil. For mechanical reasons the spider struts on Euclid are straight.

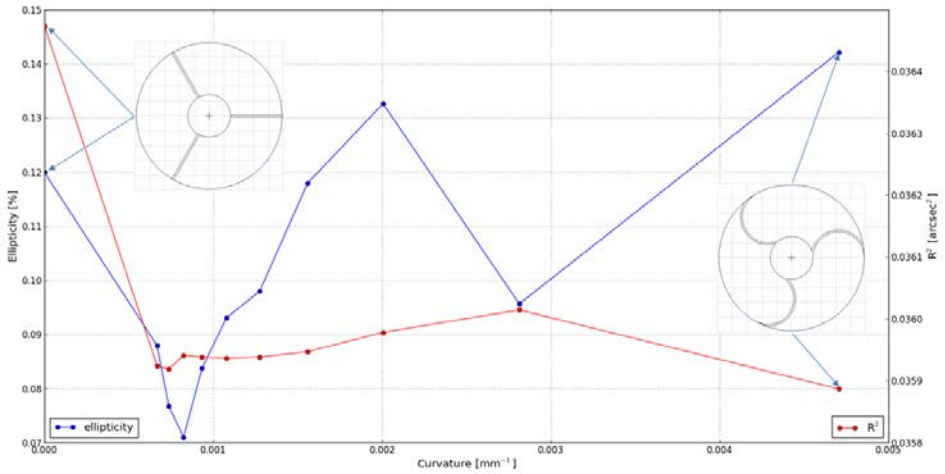

Figure 9. Impact of spider struts shape on e and R^2.

The metrics across the VIS channel FoV are derived for the telescope as designed at ambient (see Figure 10). The uniformity of the R^2 is very good (lower than 10^{-3} arcsec^2). The nominal values for R^2 are close to the specified value of 0.055 arcsec^2. The ellipticity variation across the FoV is higher but the values remain low.

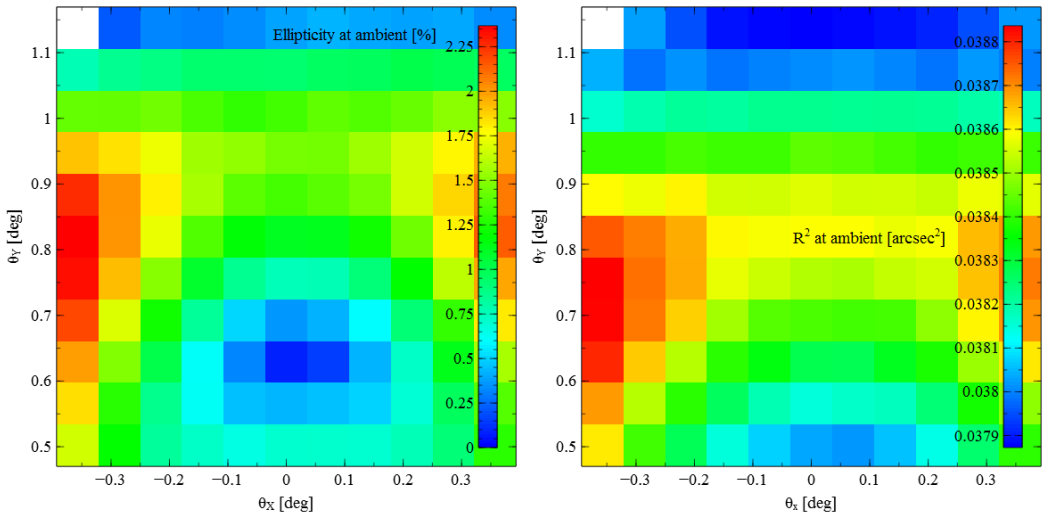

Figure 10. Nominal R^2 and e values across the VIS channel FoV at ambient.

The same analysis is performed for the telescope at cold (T=127K). The optical model only considers the rigid body motions of the mirrors. A refocusing of the M2M is performed using the WFE on 9 points evenly distributed in the VIS FoV.
The results are shown in Figure 11.

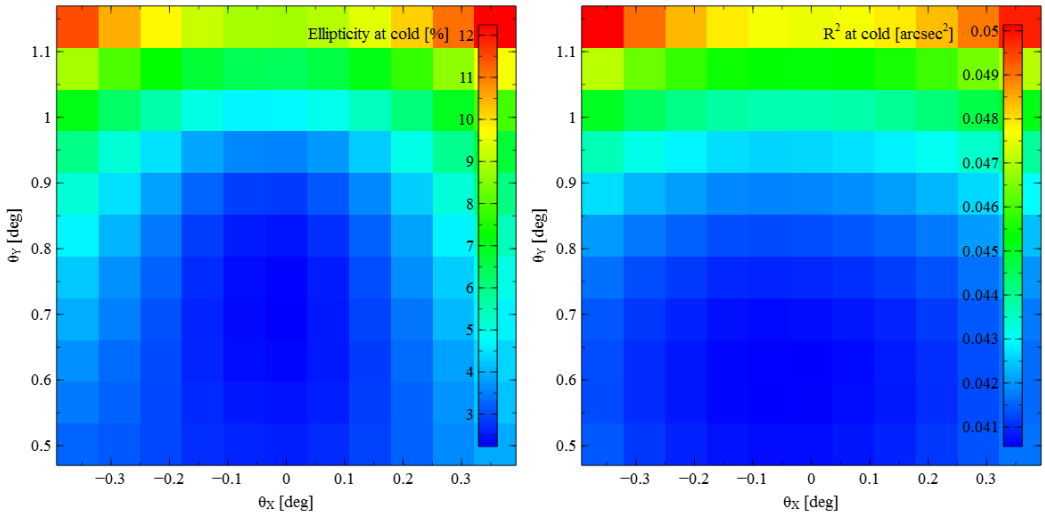

Figure 11. R^2(Right) and e(Left) across the VIS FoV at cold, after refocusing.

The FWHM at ambient and cold are derived on the same PSFs over the VIS channel FoV. The results are shown in Figure 12. After refocusing the degradation due to cool-down are partially compensated. It has to be mentioned that the refocusing method used for the purpose of this paper is not the one that will be used in-flight. The latest will be based on the measurement of R^2 and e of images of stars located at different positions within the VIS FoV.

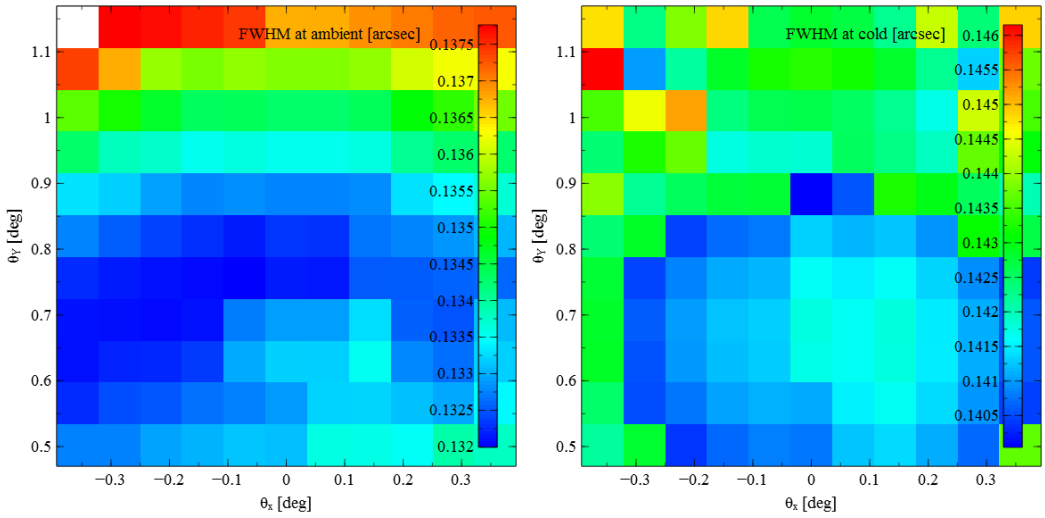

Figure 12. (Left) FWHM at ambient and (Right) FWHM at cold after refocusing across the VIS channel FoV.

3.4 The telescope image quality in NISP channel

The EE50 and EE80 radii in the focal plane of the telescope NISP channel are derived at ambient (as designed) and at cold including the mirrors rigid body motions. The mirrors and dichroic plate WFEs are not included in the optical model used to derive the EE50 and EE80 radii. The results at ambient are shown in Figure 13. For the EE50 and EE80 radii at cold, the same displacements (focus and tilts) than in section 3.3 are applied to the M2M. The results are shown in Figure 14. The results at cold seem even better than as designed. However the contribution of the mirrors and dichroic WFEs is not yet taken into account in the results.

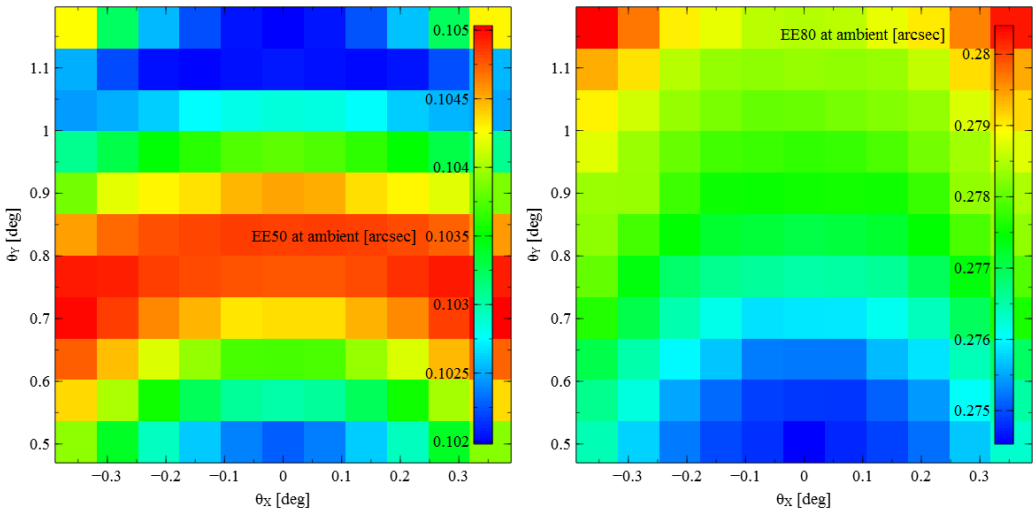

Figure 13. (Left) EE50 radii at ambient in NISP channel for λ=1033 nm. (Right) EE80 radii in NISP channel for λ=1033 nm.

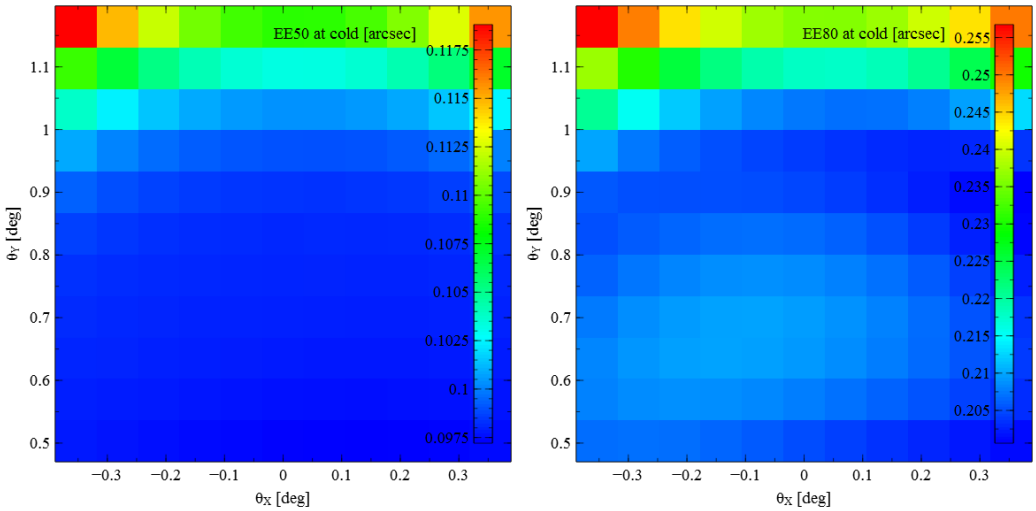

Figure 14. (Left) EE50 radii at cold in NISP channel for λ=1033 nm. (Right) EE80 radii at cold in NISP channel for λ=1033 nm.

3.5 Dichroic ghosts

The dichroic plate has a small wedge angle not sufficient to reject the ghosts in the VIS and NISP channels generated by reflections on the back face of the dichroic. The first order ghosts are critical since closer to the image and with higher irradiance. The contamination created by the ghost of a galaxy on neighboring galaxies image may have an impact on the rejection of those galaxies for the derivation of the WL signal. In Figure 15 the ghost characteristics in the VIS and NISP channels are given. The Ghost/Image includes the theoretical reflectance for the dichroic and the FOMs spectral templates. For the mirrors M1, M2 and M3 the coating is identical to the Gaia's telescope mirrors. The Ghost/Image ratio for the NISP channel is for the telescope only, the contribution of the filters and grisms in the NISP instrument are

not considered here. The first assessment of the nominal (i.e. without tolerances for the dichroic coatings and with FOMs spectral templates) average ghost ratio is 3.4e-7 in the spectral band 400 nm to 1600 nm in the VIS channel.

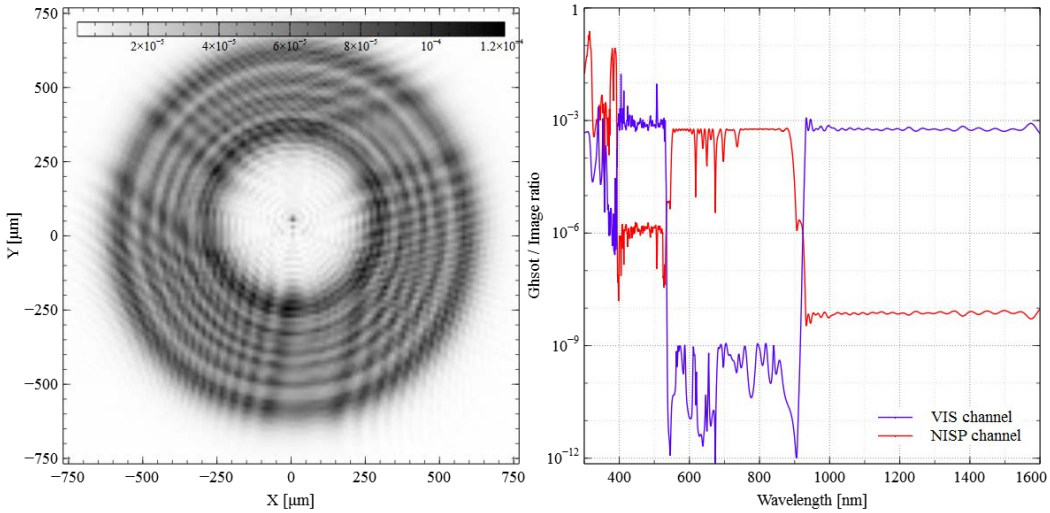

Figure 15. (Left) VIS channel first order ghost for λ=400 nm. (Right) Spectral Ghost/Image ratio for both channels.

4. THE TECHNICAL CHALLENGES

4.1 Manufacturing of critical components

The dichroic is one of the most critical components for the performances of the PLM. Its contribution to the telescope imaging performance is critical due to its location in the telescope exit pupil. During the dichroic breadboarding activities funded by ESA, the focus was put on the reduction of the WFE both in reflection and transmission due to the bi-metallic bending introduced at cryogenic temperatures by the coatings applied to the dichroic plate surfaces. For the breadboard developed by Selex Galileo, two different compensation technique were successfully used: 1) an additional layer of silicon oxide (S_iO_2) is applied between the dichroic plate substrate and the AR coating, 2) the surfaces are pre-shaped with the negative of the surface deformations expected at cold. Both techniques showed similar results for the Root Mean Square (RMS) and Peak-to-Valley (PtV) values of the WFE. The Figure 16 (resp. Figure 17) shows the measured WFE map for the breadboard with the S_iO_2 compensation layer in reflection (resp. in transmission). At T=160K, in reflection the WFE (piston, tilt removed) is 15.20 nm RMS and 15.13 nm RMS without the focus term. At T=160K, in transmission the WFE is limited to 15.38 nm RMS (resp. 14.28 nm RMS) with (resp. without) the focus term.

The feasibility of the WFE is thus demonstrated on representative breadboards. The current activities for the dichroic lead by OBJ and Amos/Schott address the challenges of an extended spectral range (starting at 300 nm instead of 550 nm for the first breadboard) and the low WFE over a diameter of 116mm in thermo-vacuum conditions. The ghost ratio must be lower than 1e-5 in reflection and 5e-3 in transmission.

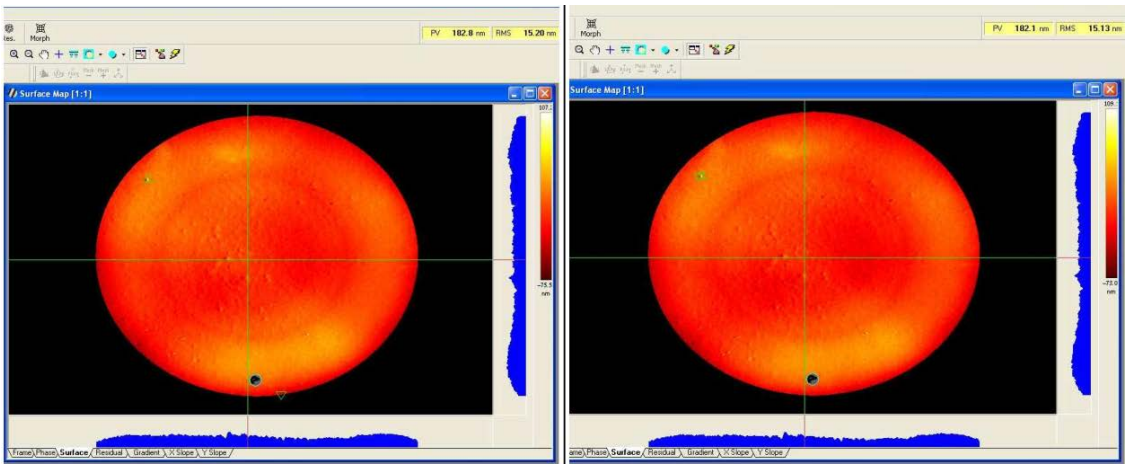

Figure 16. WFE in reflection at T=160K of the dichroic plate after dichroic and AR coatings are applied. (Left) WFE tilt & piston removed. (Right) WFE tilt, piston & focus removed.

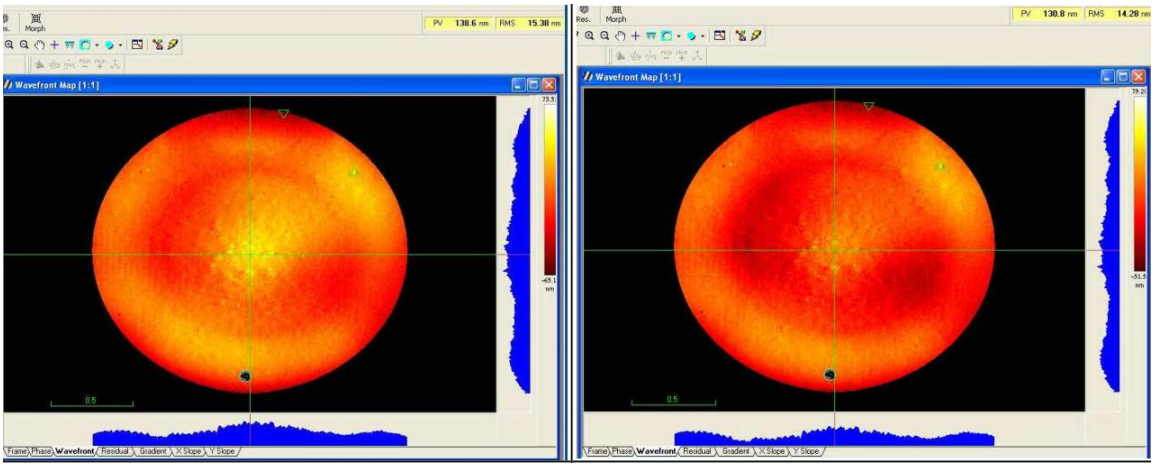

Figure 17. WFE in transmission at T=160K of the dichroic plate after dichroic and AR coatings are applied. (Left) WFE tilt & piston removed. (Right) WFE tilt, piston & focus removed.

The FOMs have spectral functionalities and help to enhance the out-of-band rejection in the VIS channel. The FOM1 and FOM2 have high-pass filter at 550 nm with a transition of 25nm. The FOM3 has a band-pass filter between 550 nm and 900 nm with transitions of 25 nm at 500 nm and 35nm at 900nm. Such coatings ought to be relatively easy on small size components, this is not the case for the FOMs. The dimensions of the coated area for FOM1 and FOM3 are 370×215 mm^2, the FOM2 dimensions are 290×226 mm^2. For each mirror, the same template applies over the entire coated area.

4.2 End-to-end testing of PLM in thermo-vacuum conditions

The PSFs in both channels must be accurately known in cryogenic conditions. An end-to-end test in thermo-vacuum conditions is foreseen as part of the PLM verification plan. For that purpose a thermo-vacuum compatible collimator with integrated light sources at different wavelengths will be developed, integrated and qualified after integration in a thermo-vacuum chamber. The highly stable and high quality collimator is by itself a challenge to develop. For the end-to-end test, the pixelated PSFs delivered by the instruments will be processed to derive all the needed metrics across the FoV of each instrument.

4.3 Straylight control

The light of a galaxy scattered by the optical surfaces and also the mechanical parts around them will illuminate pixels away from the image of this galaxy, contaminating neighboring images of galaxies. As for the ghost, if the contamination is too high the galaxies will be discarded from the analysis thus degrading the potential scientific return

for each field observed. An example if given in Figure 18 for the NISP instrument assuming a particulate contamination of 1800ppm for the NISP first lens's front surface and 900ppm for all the other surfaces of the NISP, and a micro-roughness of 1nm RMS per surface. At about 200µm away from the peak of the PSF, equivalent to 3.37 arcsec in the sky, the straylight irradiance is about 10^5 lower than the PSF peak Thus for an object of magnitude m_{AB}=8, the pixel irradiance resulting from the scattering of the light of this object is equivalent to a magnitude $m_{AB} \leq 20.5$. Hence the signal of a galaxy with a magnitude $m_{AB} \geq 20.5$ located within 3.37 arcsec from the scattered object might be contaminated by straylight to the point it would be discarded. This has a direct impact on the total area of the sky actually useful within the duration of the Euclid mission.

A significant effort is currently put on the identification, quantification and mitigation of any sources of straylight in-field and out-of-field. This work involves the industrial partners, ESA and the Euclid scientific consortium. Several sources internal to the telescope have been identified, however other sources (primary or secondary) can be generated by multiple scattering from the instruments optical and mechanical parts. All potential disturbances must be accounted for and quantified. In addition of this work, as part of the telescope verification, straylight tests in and out-of-field will be performed by Airbus.

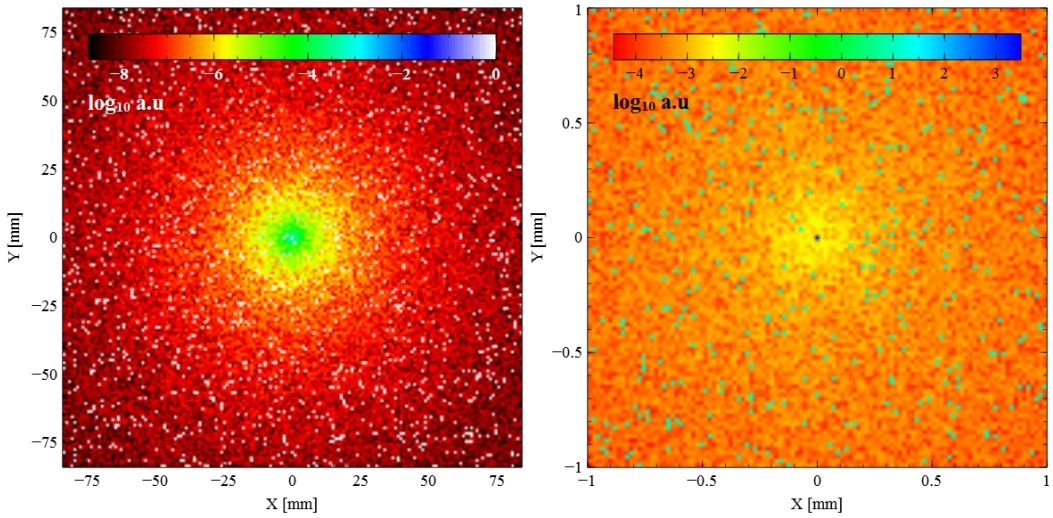

Figure 18. (Left) Scattered light including particulate contamination and surfaces roughness over the NISP instrument focal plane. (Right) Zoom around the PSF located at the center of the NISP instrument FoV.

5. CONCLUSIONS

The scientific objectives of the Euclid mission are challenging. The complexity of the topics addressed (dark matter and dark energy) is reflected in the specification, design, manufacturing, integration and testing phases of the Euclid PLM.

The optical design of the telescope is now frozen. The resulting nominal performances at ambient and at cold are within the specifications for both VIS and NISP channels. The first assessment of performance shows the high quality of imaging over the VIS and NISP instruments FoV both at ambient and at operational temperatures. For the latest case, the rigid body motion of the mirrors have a negative impact on the PSF metrics. However, most of the degradation of the image quality is compensated by refocusing and tilting the M2 mirror.

Several critical points are currently being addressed. In particular the spectral performances of the dichroic and FOMs will be known in the next months. The feasibility of the dichroic has been already demonstrated during an early breadboarding activity. The same cannot be said for the development of the FOMs. The development of such large components is an interesting challenge to be addressed by the European industry.

The straylight assessment is an on-going work. Its impact on the final scientific results will be supported not only by brute force simulations but also by testing at telescope and components level. A dedicated straylight working group was set-up to follow this particular topic during the different phases of development of the Euclid spacecraft.

ACKNOWLEDGEMENTS

The authors would like to thank our esteemed colleague Bernd Harnisch from ESA/ESTEC-TEC-MMO for making available the data on the dichroic breadboarding activity.

REFERENCES

[1] ESA, "Euclid Mapping the geometry of the dark universe", ESA/SRE(2011)12, July 2011, http://sci.esa.int/euclid/48983-euclid-definition-study-report-esa-sre-2011-12/#.
[2] Murdin, P., [Encyclopedia of Astronomy and Astrophysics], Nature Publishing Group, Institute of Physics Publishing, (2001).
[3] http://sci.esa.int/euclid/42267-science/
[4] F. Grupp, E. Prieto, N. Geis, A. Bode, R. Katterloher, R. Grange, V. Junk, and R. Bender, "The optical baseline concept of the NISP near infrared spectrometer and photometer on board of the ESA/EUCLID satellite", Proc. SPIE 8442, p. 84420X–84420X–11 (2012).
[5] M. Cropper, H. Hoekstra, T. Kitching, R. Massey, J. Amiaux, L. Miller, Y. Mellier, J. Rhodes, B. Rowe, S. Pires, C. Saxton, and R. Scaramella, "Defining a weak lensing experiment in space", *arXiv:1210.7691 [astro-ph]* (2012).
[6] http://smsc.cnes.fr/EUCLID/Fr/GP_nisp.htm